CHEMISTRY OF MATERIALS

Open Access

pubs.acs.org/cm

Article

Self-Sorting in Multicomponent Supramolecular Gels Using Different Assembly Triggers and Calcium Ion-Induced Diffusion Patterning

Chayanan Tangsombun and David K. Smith*

Cite This: https://doi.org/10.1021/acs.chemmater.4c00183

Read Online

ACCESS | Metrics & More | Article Recommendations | Supporting Information

ABSTRACT: This paper investigates self-sorting and triggered assembly of multicomponent gels that combine sorbitol-based low-molecular-weight gelator (LMWG) DBS-CONHNH$_2$ and peptide-based LMWG Nap-FF, with the assembly of Nap-FF being triggered either using glucono-δ-lactone (GdL) to lower pH or $CaCl_2$. Changing triggers alters the way Nap-FF assembles on the molecular scale either as its acid form or its calcium salt, leading to different nanoscale networks and rheological behaviors. The choice of trigger impacts the properties of the two-component gels formed with DBS-CONHNH$_2$. Using either trigger, the LMWGs self-sort on the molecular level into their own distinct assemblies. However, when using a GdL trigger, the sheet-like Nap-FF assemblies encourage DBS-CONHNH$_2$ assembly, with the two assemblies interacting with one another on a network level as a result of interactions between the acylhydrazide and the carboxylic acid. Conversely, when using a $CaCl_2$ trigger, the two fibrillar assemblies are independent of one another on the network level, with the carboxylic acid being bound to calcium in the form of its carboxylate salt, and unable to interact with DBS-CONHNH$_2$. As such, GdL-triggering leads to molecular-level self-sorting and network-level coassembly, while $CaCl_2$-triggering leads to both molecular-level and network-level self-sorting. Injecting the $CaCl_2$ trigger into a preformed DBS-CONHNH$_2$ gel, followed by its diffusion, creates dynamic, evolving, spatially-resolved self-sorted multicomponent gels, with stiffnesses differing by 2 orders of magnitude in different domains. Given the mild, biocompatible nature of $CaCl_2$, it is suggested that this calcium ion diffusion approach to spatiotemporally resolved patterning of multidomain gels may have future relevance in cell-based studies.

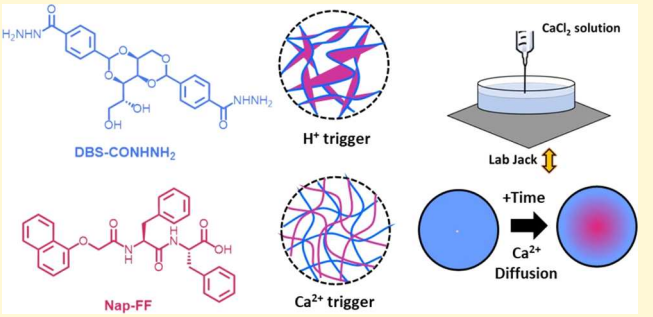

INTRODUCTION

Supramolecular gels based on low-molecular-weight gelators (LMWGs) that self-assemble through noncovalent interactions to immobilize bulk solvents even at relatively low loadings are an important class of nanomaterial.[1−3] By programming molecular structure, it is possible to impact the mode of assembly, which can be triggered by a variety of different processes.[4,5] Gels have a wide range of applications, from catalysis and environmental remediation to drug delivery and tissue engineering, meaning that in addition to fundamental interest in self-assembly pathways, they have potential in next-generation technologies.[1,6−9]

Given that self-assembly is a simple, bottom-up fabrication method, it is straightforward to create multicomponent gels by mixing LMWGs.[10−12] In such multicomponent systems, self-sorting occurs when individual gelators independently assemble into their own individual nanostructures; coassembly means individual LMWGs assemble with one another into a new combined nanostructure, and disruptive assembly means the two LMWGs limit one another's ability to self-assemble. Self-sorting is of particular use because it allows gels to be programmed by the molecular structures of the LMWGs, with each gelator expressing its own properties in the final material.[13−22] Importantly, however, consideration should also be made beyond the molecular-level assembly process. For example, although a system may self-sort on the molecular scale, the resulting fibers may preferentially self-interact, interact with one another, or form no specific interactions at all. Each outcome can lead to gels with different microstructures and properties. Such studies are of very high potential value, as they help understand a hierarchical assembly level that is difficult to probe, but as yet, they have only been rarely performed.[23−25] Understanding multicomponent assembly across all length scales and moving beyond a simple focus on molecular-level assembly remains an important, largely

Received: January 22, 2024
Revised: May 3, 2024
Accepted: May 6, 2024

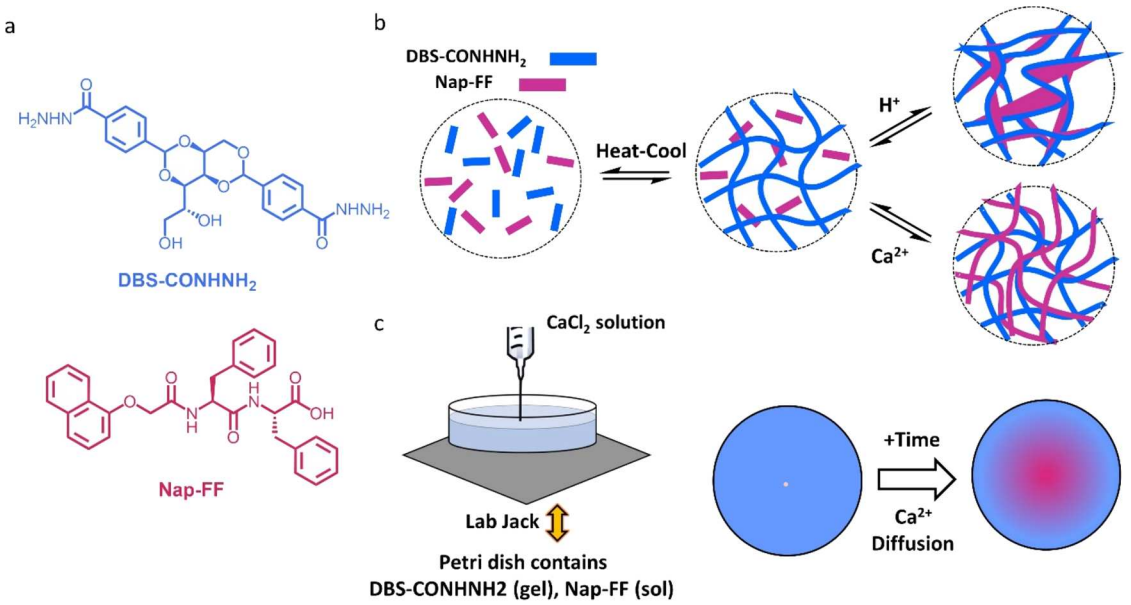

Figure 1. (a) Structures of LMWGs investigated in this paper, DBS-CONHNH$_2$ and Nap-FF. (b) Schematic of multicomponent assembly triggered by a heat/cool cycle to assemble DBS-CONHNH$_2$ combined with either H^+ or Ca^{2+} to assemble Nap-FF, with the choice of trigger leading to different outcomes. (c) Schematic showing the use of injected Ca^{2+} as a diffusing trigger to assemble Nap-FF within a preformed network of DBS-CONHNH$_2$.

unmet challenge in supramolecular gel science.[26] It is evident that by controlling each level of the hierarchical assembly process, it should be possible to gain a greater degree of control over multicomponent gel-phase materials.

We became interested in assembling gelators with divergent chemical structures with a longer-term interest in developing biologically relevant multicomponent materials. Specifically, we want to endow our stem cell-compatible sugar-based gelator, DBS-CONHNH$_2$ (Figure 1),[27−29] with additional functions. We have previously combined this LMWG with pH-responsive DBS-COOH;[30] however, the pK_a of DBS-COOH is 5.4, and assembly only occurs below this pH value, which is not ideal for biological applications. With the long-term goal of raising the stability of the second network in biological media, a literature survey identified peptide-based gelator Nap-FF (Figure 1A), which has a pK_a value of 6.8, as a potentially interesting LMWG to combine with DBS-CONHNH$_2$.[31,32] The pK_a of Nap-FF is higher than the typical C-terminus of a peptide due to hydrophobically driven self-assembly.[33,34] Peptide gelators of this type are well understood through the careful work of a number of researchers.[35−41] In particular, Adams and co-workers have characterized multicomponent systems, gaining understanding across multiple length scales.[42−45] However, a combination of this peptide LMWG with other gelators having very different chemical structures remains rare. We also noted that the assembly of this class of peptide gel could be triggered by calcium ions,[46−51] not possible for our own acid-functionalized LMWG (DBS-COOH) and realized that this opened new possibilities in terms of gel patterning that might be relevant in biological systems. Furthermore, calcium ions had not previously been used to trigger multicomponent gel systems.

We therefore targeted multicomponent systems based on DBS-CONHNH$_2$/Nap-FF (Figure 1B) and aimed to compare and contrast the use of H^+ and Ca^{2+} to trigger assembly, understanding how the two LMWGs impacted on one another's assembly and how using different triggers impacted on multicomponent assembly. Furthermore, we wanted to explore the considerable potential of Ca^{2+} to create patterned gels (Figure 1c). There has been emerging interest in shaping and patterning supramolecular gels,[52,53] and diffusion can be an effective way of achieving dynamic patterning.[54,55] For example, some studies have used H^+ diffusion to trigger gel assembly with spatial and temporal resolution.[56−61] We previously achieved spatiotemporally resolved patterning of DBS-COOH and DBS-CONHNH$_2$ based on acid diffusion.[62−64] We reasoned that replacing DBS-COOH with Nap-FF may not only raise the pK_a value to useful levels but also enable calcium ion diffusion to direct gel assembly, offering a potentially biocompatible method for generating patterned multidomain materials with potential future applications in tissue engineering.

EXPERIMENTAL SECTION

Materials and General Methods. Chemicals were purchased from standard chemical suppliers for synthesis and analysis. Nap-FF was synthesized from 1-naphthol by applying a stepwise protocol, as previously described by Adams and co-workers.[31,65,66] DBS-CONHNH$_2$ was prepared through a simple two-step synthesis, as described in our previous reports.[27] Characterization data were in agreement with previous reports. ^{1}H NMR spectra were recorded on a Jeol 400 spectrometer (^{1}H 400 MHz). Samples were prepared as solutions in deuterated NMR solvents (DMSO-d_6 or D_2O), and chemical shifts (δ) are quoted in parts per million (ppm) referenced to residual solvent. A Bruker 500 (^{1}H 500 MHz) was used for kinetics experiments. IR spectra were recorded on a PerkinElmer Spectrum Two FT-IR spectrometer. Fluorescence spectra were recorded using a Hitachi F-4500 fluorescence spectrophotometer. Circular dichroism (CD) measurements were carried out using a Jasco J-1500 spectrophotometer. Transmission electron microscopy (TEM) images were recorded on a FEI Tecnai 12 G^2 fitted with a CCD camera. Scanning electron microscopy (SEM) images were obtained from a Jeol JSM 6490LV scanning electron microscope. T_{gel} values were obtained by tube inversion using a high-precision thermoregulated oil bath. Rheological measurements were recorded using a Malvern

https://doi.org/10.1021/acs.chemmater.4c00183
Chem. Mater. XXXX, XXX, XXX−XXX

Instruments Kinexus Pro+ rheometer fitted with a 20 mm parallel plate geometry.

Gel Fabrication. *DBS-CONHNH$_2$ Gels.* DBS-CONHNH$_2$ (3 mg, 0.3 wt %/vol) was suspended in water (1 mL). The mixture was sonicated and then heated with a heat gun until complete dissolution. This was left undisturbed overnight to allow gel formation.

Nap-FF Hydrogel via pH-Switching. A known mass of Nap-FF was weighed into a sample vial. A solution of NaOH (0.5 M, 1.3 equiv) and water (1 mL total volume) was added. The suspension was sonicated until complete dissolution, and the pH of the gelator solution was measured to be around 10. This solution was transferred into another vial containing glucono-δ-lactone (GdL, 8 mg, 0.8 wt %/vol), followed by shaking. Samples were left undisturbed overnight to allow gel formation.

Nap-FF Hydrogels via Calcium Addition. A known mass of Nap-FF was weighed into a sample vial. A solution of NaOH (0.5 M, 1.3 equiv) and water (1 mL total volume) was added. The suspension was sonicated until complete dissolution, and the pH of the gelator solution was measured to be around 10. The solution was transferred to a new sample vial containing $CaCl_2$ solution (5 wt %/vol, 0.07 mL) as quickly as possible to aid mixing and then left to stand to form a gel.

DBS-CONHNH$_2$/ Nap-FF Hydrogels via pH-Switching. A known mass of DBS-CONHNH$_2$ (0.15 or 0.3 wt %/vol) was weighed into a vial, and different concentrations of the basified Nap-FF solution described above (0.15, 0.3, or 0.5 wt %/vol, 1 mL) were then added. The mixture was sonicated for 5 min and then heated with a heat gun until complete dissolution. The hot solution was transferred into another vial containing GdL (8 mg, 0.8 wt %/vol) and left undisturbed overnight to allow gel formation.

DBS-CONHNH$_2$/Nap-FF Hydrogels via Calcium Addition. A known mass of DBS-CONHNH$_2$ (0.15 or 0.3 wt %/vol) was weighed into a vial, and different concentrations of the basified Nap-FF solution described above (0.15, 0.3, or 0.5 wt %/vol, 1 mL final total volume) were then added. The mixture was sonicated for 5 min and then heated with a heat gun until complete dissolution. The hot solution was then transferred to a vial containing $CaCl_2$ (5 wt %/vol, 70 μL) and then left to stand to form a gel.

Patterning DBS-CONHNH$_2$/Nap-FF Hydrogels via Calcium Diffusion. (i) Gel preparation in a Petri dish: Nap-FF (19 mg, 0.3 wt %/vol, 6.5 mL total) was dissolved in NaOH (0.5 M, 1.3 equiv) and water. The Nap-FF solution was mixed with DBS-CONHNH$_2$ (19 mg, 0.3 wt %/vol) and bromothymol blue or thymol blue (10 μL, 1% in EtOH). The mixture was sonicated, heated, and poured into a Petri dish (3.5 cm diameter). This was allowed to cool and left overnight, giving a gel thickness of ca. 0.7 cm. A $CaCl_2$ solution (15 μL, 2 M = 0.03 mmol) or water (15 μL) was injected using a glass syringe, with a lab jack being used to raise and lower the Petri dish. (ii) Gel preparation in a tray: Nap-FF (36 mg, 0.3 wt %/vol, 12 mL total) was dissolved in NaOH (0.5 M, 1.3 equiv) and water. The Nap-FF solution (6 mL, 0.3 wt %/vol) was added into two vials that each contained DBS-CONHNH$_2$ (18 mg, 0.3 wt %/vol). The mixture was sonicated, and each vial was simultaneously heated with a heat gun. The hot solutions from both vials were then transferred into a 5 × 5 cm square tray. The tray was left undisturbed to cool overnight, forming a gel with a thickness of 0.5 cm. A $CaCl_2$ solution (10 μL, 3 M = 0.03 mmol or 10 μL, 6 M = 0.06 mmol) was injected using a glass syringe, with a lab jack being used to raise and lower the tray.

Gel Analysis Procedures. *NMR Studies of Nap-FF Gelation Triggered via pH Change or Calcium Addition.* A suspension of Nap-FF (0.3 wt %/vol) in D_2O (1 mL) was dissolved by the addition of NaOD (30 μL, 0.5 M, 1.3 equiv) and then sonicated until complete dissolution. The solution of Nap-FF was diluted with D_2O to give the desired concentrations. The solution (0.7 mL) was then transferred to a vial containing MeCN (2 μL). The NMR spectrum of "mobile" Nap-FF was then recorded. In addition, Nap-FF solution (0.15 wt %/vol, 0.7 mL) was added to a vial containing GdL (5.6 mg, 0.8 wt %/vol) and dimethylsulfoxide (DMSO) (2 μL). This was then transferred to an NMR tube, and spectra were recorded after 24 h. Alternatively, the mobile Nap-FF was added to an NMR tube containing a calcium chloride solution (5 wt %/vol in D_2O, 0.07 mL) and DMSO (2 μL). After 24 h, the ^{1}H NMR spectra were recorded.

NMR Studies of DBS-CONHNH$_2$/Nap-FF Multicomponent Hydrogels. The "mobile" basified Nap-FF solution (0.15 or 0.10 wt %/vol) was transferred to a vial containing DBS-CONHNH$_2$ (0.15, 0.2% or 0.3 wt %/vol). The mixture was heated until complete dissolution. DMSO (2 μL) and GdL (5.6 mg, 0.8 wt %/vol) were added into the hot gelator solution (0.7 mL), and then this was transferred into an NMR tube. After 24 h, the ^{1}H NMR spectrum was recorded. For Ca-triggered gelation, the hot solution of DBS-CONHNH$_2$/Nap-FF was transferred to an NMR tube containing a calcium chloride solution (5 wt %/vol in D_2O, 0.07 mL) and DMSO (2 μL). The ^{1}H NMR spectra were recorded after 24 h.

NMR Studies of pH-Responsive DBS-CONHNH$_2$/Nap-FF Multicomponent Hydrogels. Multicomponent gels (0.5 mL) induced by GdL were prepared in NMR tubes, as described in the section above. After 24 h, ^{1}H NMR spectra of the multicomponent gels were recorded. A solution of NaOD (40 μL, 0.5 M) was then added to the top of the gel to disassemble the Nap-FF network, and after a further period of time, a solution of GdL (8 mg in 0.1 mL D_2O) was subsequently added to reform the Nap-FF network. The ^{1}H NMR spectrum was recorded for each addition. The percentage of mobile components was calculated by comparison of the integrals of Nap-FF aromatic peaks (δ = 8.13 or 6.65 ppm) and DBS-CONHNH$_2$ peak (δ = 5.90 ppm) with that of the DMSO internal standard (δ = 2.74 ppm).

NMR Kinetic Studies of Nap-FF Gelation Triggered by a pH Change or Calcium Addition. A suspension of Nap-FF (1.5 mg, 0.15 wt %/vol) in D_2O (1 mL total) was dissolved by the addition of NaOD (10 μL, 0.5 M) and then sonicated until complete dissolution. The mobile Nap-FF (0.7 mL, 0.15 wt %/vol) was transferred to a vial containing GdL (5.6 mg, 0.8 wt %/vol) and DMSO (1.4 μL), followed by shaking. This was then quickly transferred to an NMR tube. The NMR spectra of mobile Nap-FF were then recorded immediately, every 10 min for 2 h, and every 30 min for 10 h. Alternatively, the mobile Nap-FF (0.7 mL, 0.15 wt %/vol) was added to an NMR tube containing a calcium chloride solution (5 wt %/vol in D_2O, 0.07 mL) and DMSO (1.4 μL). The NMR spectra were then recorded at time intervals as described above.

NMR Kinetic Studies of DBS-CONHNH$_2$/Nap-FF Triggered by a pH Change or Calcium Addition. The "mobile" Nap-FF (0.7 mL, 0.15 wt %/vol) was transferred to the vial containing DBS-CONHNH$_2$ (2.1 mg). The mixture was heated until complete dissolution. The hot gelator solution was added into DMSO (1.4 μL) and GdL (5.6 mg, 0.8 wt %/vol), followed by shaking. This was then quickly transferred to an NMR tube. The NMR spectra of mobile Nap-FF were then recorded immediately, every 10 min for 2 h, and every 30 min for 10. For Ca^{2+}-triggered gelation, the hot solution of DBS-CONHNH$_2$/Nap-FF (0.7 mL, 0.3 wt %/vol of DBS-CONHNH$_2$ and 0.15 wt %/vol of Nap-FF) was transferred to an NMR tube containing a calcium solution (5 wt %/vol in D_2O, 0.07 mL) and DMSO (1.4 μL). The NMR spectra were then recorded at time intervals as described above.

NMR Quantification of the Self-Assembly of Nap-FF Triggered by CaCl$_2$ Diffusion. The gel without an indicator was prepared in a 3.5 cm Petri dish as described previously, but using D_2O and NaOD. A $CaCl_2$ solution prepared in D_2O (15 μL, 2 M = 0.03 mmol) was injected into the middle of the dish. At 1 h, 3 h, 6 h, and 24 h, an aliquot (100 μL) of gel was taken at different distances (0−5.8 mm, 5.8−11.6 mm, and 11.6−17.5 mm) from the injection point using a cut plastic syringe and then gently transferred to a vial containing D_2O (0.6 mL). DMSO (2 μL) was added as an internal standard. After that, this was transferred to an NMR tube with the least possible disturbance, and the ^{1}H NMR spectrum was recorded. The percentage of mobile component (Figure S12) was calculated by comparison of the integrals of Nap-FF aromatic peak (δ = 8.16 ppm) with that of the DMSO peak (δ = 2.71 ppm).

Fluorescence Spectroscopy. To prepare the DBS-CONHNH$_2$ hydrogel, a suspension of DBS-CONHNH$_2$ (6 mg, 0.3 wt %/vol) in water was sonicated and heated to a clear solution. The hot

https://doi.org/10.1021/acs.chemmater.4c00183
Chem. Mater. XXXX, XXX, XXX−XXX

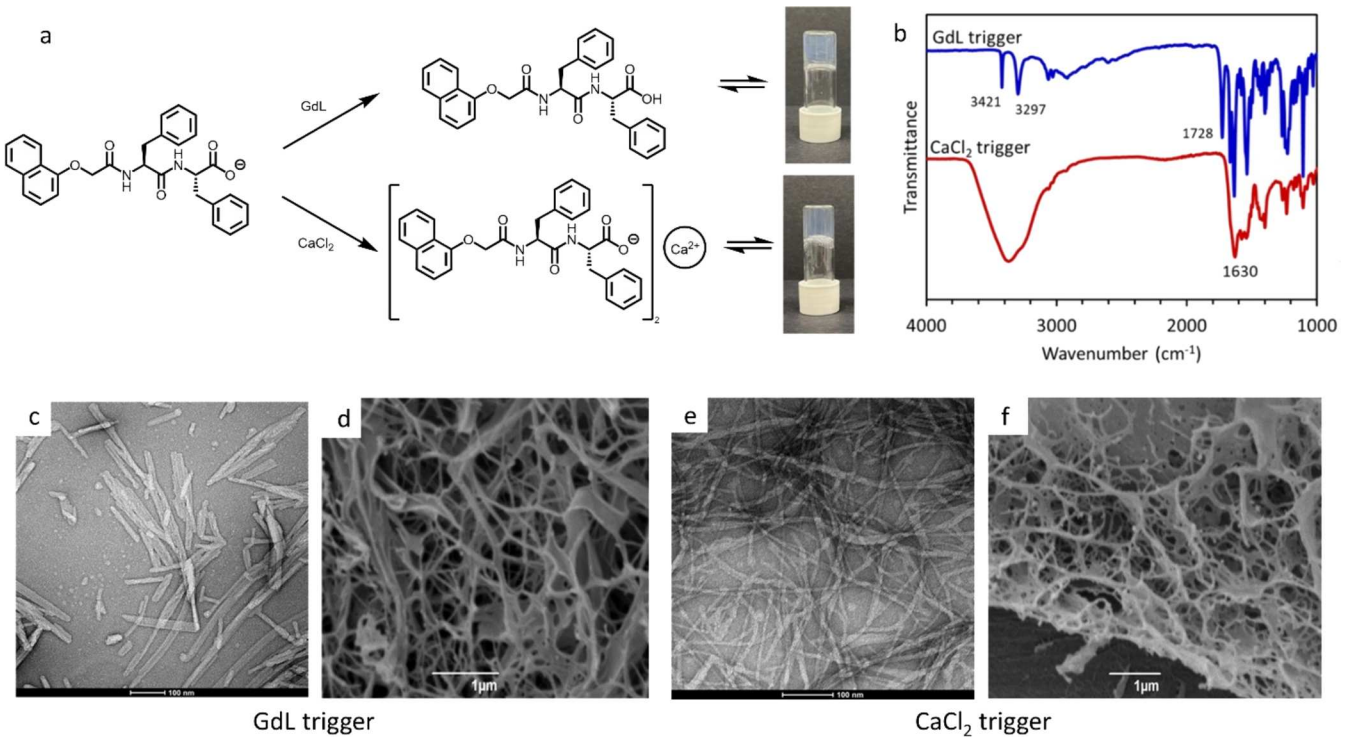

Figure 2. (a) Molecular structure of deprotonated Nap-FF, scheme indicating how GdL or $CaCl_2$ trigger gel formation in different ways, including photographs of the Nap-FF gels formed by GdL or $CaCl_2$ triggers. (b) IR spectra of Nap-FF xerogels formed with GdL or $CaCl_2$ triggers. (c) TEM image of Nap-FF triggered by GdL, scale bar = 100 nm. (d) SEM image of Nap-FF triggered by GdL, scale bar = 1 μm. (e) TEM image of Nap-FF triggered by $CaCl_2$; scale bar = 100 nm. (f) SEM image of Nap-FF triggered by $CaCl_2$, scale bar = 1 μm.

solution was then transferred to a cuvette with a path length of 10 mm and allowed to form a gel overnight. For DBS-$CONHNH_2$/Nap-FF gel, a suspension of DBS-$CONHNH_2$ (6 mg, 0.3 wt %/vol) in a basified solution of Nap-FF (2 mL, 0.3 wt %/vol) was sonicated and heated until dissolution. This solution was loaded into a cuvette containing GdL (0.8 wt %/vol) and then allowed to form a gel overnight. In the case of the multicomponent gel in which Nap-FF was assembled by adding calcium chloride, the hot solution of DBS-$CONHNH_2$/Nap-FF was transferred to a cuvette containing aqueous calcium chloride (5 wt %/vol, 0.140 mL) and then allowed to form a gel overnight to give DBS-$CONHNH_2$/Nap-FF (0.3 wt %/vol of DBS-$CONHNH_2$ and 0.3 wt %/vol of Nap-FF, final volume of 2 mL). The fluorescence spectra of DBS-$CONHNH_2$ and DBS-$CONHNH_2$/Nap-FF gels were recorded, exciting at a wavelength of 280 nm.

Time-Resolved Fluorescence Spectroscopy. Basified Nap-FF solution (2 mL, 0.3 wt %/vol) was loaded into a cuvette of 10 mm path length, and the first fluorescence spectrum was collected with excitation at 280 nm. GdL (16 mg, 0.8 wt %/vol) was added. In the case of calcium-induced gelation, the solution of calcium chloride (5 wt %/vol, 0.070 mL) was added. Emission spectra were measured every 10 min for 2 h, and subsequently at 24 h at room temperature, with excitation at 280 nm. The emission spectra were recorded between 285 and 800 nm. The slit width of both excitation and emission was set to 10 nm; scan speed was 240 nm/min.

Infrared Spectroscopy. Gels were prepared in vials by applying the methods described above. The gels were dried in vacuum prior to analysis. The xerogels were placed into the infrared spectrophotometer and IR spectra recorded from 4000 to 450 cm^{-1}.

CD Spectroscopy. CD spectra were measured at 20 °C on a Jasco J-1500 spectropolarimeter between 180 and 400 nm using the following settings: data Pitch = 0.5 nm, bandwidth = 1.00 nm, scanning mode = continuous, scan speed = 100 nm/min, and accumulation = 2. A CD cuvette (quartz, path length 1 mm) was used.

CD Studies of DBS-$CONHNH_2$. A known mass of DBS-$CONHNH_2$ (1 mg) was weighed into a vial, and water (10 mL for 0.01 wt %/vol or 5 mL for 0.02 wt %/vol) was then added. The mixture was sonicated for 5 min and then heated with a heat gun until complete dissolution. The solution (0.4 mL) was transferred to a CD cuvette and left for 24 h before the spectra were recorded.

CD Studies of Nap-FF. Nap-FF (1.5 mg, 0.15 wt %/vol) was suspended in NaOH (10 μL, 0.5 M) and pure water (1 mL total). The suspension was sonicated until complete dissolution. The Nap-FF solution (0.01 or 0.02 wt %/vol, 2 mL) was prepared by diluting the Nap-FF solution (0.15 wt %/vol) with pure water. The Nap-FF solution (0.01 or 0.02 wt %/vol, 0.4 mL) was then added to a vial containing GdL (3.2 mg) or HCl (1M, 20 μL), followed by shaking. This solution was then transferred to a CD cuvette and left for 24 h before the spectra were recorded. Alternatively, the Nap-FF solution (0.01 or 0.02 wt %/vol, 0.4 mL) was then added to a CD cuvette containing $CaCl_2$ (5 wt %/vol, 20 μL) and left for 24 h before the spectra were recorded.

CD Studies of DBS-$CONHNH_2$/Nap-FF. A Nap-FF solution (10 mL of 0.01 wt %/vol or 5 mL of 0.02 wt %/vol) was added to a vial containing DBS-$CONHNH_2$ (1 mg), sonicated for 5 min, and heated with a heat gun until complete dissolution. The hot gelator solution (0.01 or 0.02 wt %/vol of each LMWGs, 0.4 mL) was transferred to a vial containing GdL (3.2 mg) or HCl (1M, 20 μL), followed by shaking, quickly transferred to a CD cuvette, and left for 24 h before the spectra were recorded. Alternatively, the hot gelator solution (0.01 or 0.02 wt %/vol of each LMWGs, 0.4 mL) was transferred to a CD cuvette containing $CaCl_2$ (5 wt %/vol, 20 μL) and left for 24 h before the spectra were recorded.

Time-Resolved CD Spectroscopy. All samples were prepared as described above. 400 μL of the solution was transferred to a CD cuvette, and the spectra were recorded immediately and then every 10 min for 2.5 h, and again at 24 h for GdL-induced assembly or every 10 min for 1.5 h, and then at 24 h for calcium-induced assembly.

Transmission Electron Microscopy (TEM). Gel samples in vials were prepared as described above. For patterned gels, samples were prepared in a glass tray as described above, and calcium chloride solution (3 M, 10 μL) was injected into the preformed DBS-$CONHNH_2$ gel. After 2.5 h, the inner and outer domains were cut

https://doi.org/10.1021/acs.chemmater.4c00183
Chem. Mater. XXXX, XXX, XXX−XXX

using a bottomless vial and carefully transferred to a Petri dish. TEM images were obtained by placing a small amount of each sample on a copper grid. The excess sample was removed with filter paper and allowed to set for 5 min. A negative stain (1% uranyl acetate) was then added. Before images were taken, the samples were left to rest for 30 min. Fiber widths were measured from TEM images using ImageJ Software.

Scanning Electron Microscopy (SEM). Samples were frozen by immersion into slushy liquid nitrogen and then transferred to a Polaron E5380 freeze drier unit and processed at −60 °C for about 4 h. The samples were then allowed to warm up slowly and mounted onto SEM stubs. The mounted samples were sputter coated with 5 nm of gold−palladium and then imaged on Jeol JSM 6490LV SEM operating at an accelerating voltage of 5 kV.

Thermal Stability. Gels were prepared as described above in 7 mL vials (diameter = 2 cm, height = 6 cm) and left overnight, allowing gel formation. They were placed in a high-precision thermoregulated oil bath with an initial temperature of 25 °C. The temperature was then increased by 1 °C/min until 100 °C. The gels were checked by the tube inversion method every minute. The temperature (T_{gel}) was recorded when the gel began to run down the side of the vial. These experiments were repeated three times, and the average T_{gel} was recorded. Errors are estimated at ±2 °C.

Rheology for Gels in Vials. Gels were prepared as described above (1 mL volume), with the amount of GdL as a pH trigger being 0.8 wt %/vol in a bottomless vial attached to a glass Petri dish and left overnight to ensure complete gel formation. The gels were then transferred and placed on the rheometer using a spatula. Measurements were carried out at 25 °C using a 20 mm parallel plate and a gap of 2.5 mm. Amplitude sweep was performed in the range of 0.01−100% strain at a 1 Hz frequency. The frequency sweep was performed between 0.1 and 100 Hz using a shear strain of 0.15%. For reproducibility, experiments were repeated three times, and average data were used to plot the graphs.

Rheology Studies for Gels Patterned by Calcium Diffusion. The gel was prepared in a 5 × 5 cm tray as described above. A $CaCl_2$ solution was injected into the tray with two injection points in bottom left and top right corners. When the patterned gel domain had a diameter ca. 2 cm (~2.5 h), bottomless vials were used to cut the gel at the inner domain and the outer domain. The cut gel was transferred to Petri dishes and then to the rheometer. Measurements were carried out as described above.

RESULTS AND DISCUSSION

The low-molecular-weight gelator (LMWG), DBS-$CONHNH_2$, was prepared by our well-established simple two-step synthesis.[27] Dipeptide LMWG, Nap-FF, was synthesized using the published method starting from commercially available 1-naphthol and applying standard peptide synthesis methods. All molecules were fully characterized, with data in agreement with previous studies.[27,31,65,66] The formation of Nap-FF hydrogels can be achieved using two different approaches: (i) slowly lowering pH with glucono-δ-lactone (GdL) or (ii) adding calcium ions to form the calcium salt.[46,67] Although these gels have been reported before, we briefly investigated each triggering approach to benchmark our later results, before going onto compare their use in the formation of multicomponent gels with DBS-$CONHNH_2$.

Comparing Gel Formation from Nap-FF Using GdL or $CaCl_2$. Nap-FF formed translucent gels via pH-switching with a GdL trigger (Figure 2a). The gels formed slowly as GdL hydrolyzed and had a minimum gelation concentration (MGC) of 0.06 wt %/vol, with a final pH value of 4.1. The gels exhibited metastability over extended storage periods (days), converting into a turbid gel. All gels were therefore stored for a controlled period of time (12 h) prior to study. This type of metastability has previously been discussed by Adams and co-workers.[65,68,69] In contrast, gels triggered by the addition of aqueous calcium chloride (5 wt %/vol) rapidly gave transparent hydrogels (Figure 2a), visually different from the translucent gels triggered by GdL addition, with a final pH value of ca. 7.0. Furthermore, the $CaCl_2$-triggered Nap-FF hydrogels appeared to be stable over time.

The assembly of Nap-FF was monitored *in situ* using ^{1}H NMR spectroscopy. The maximum amount of Nap-FF that gave distinctive sharp peaks in the basic solution in the aromatic region was 0.15 wt %/vol. Above this value, the peaks broadened as a result of Nap-FF forming worm-like micelles, consistent with previous reports.[67,70] On addition of GdL or $CaCl_2$, the peaks for Nap-FF disappeared as the gel network assembled (Figures S5 and S6). Molecules present in the liquid-like solution phase exhibit sharp NMR peaks, whereas those immobilized within solid-like gel assemblies are broadened and not observable by NMR.[71,72] More detailed analysis indicated that with a GdL trigger, there was a rapid assembly of Nap-FF, possibly caused by residual NaOH inducing GdL hydrolysis, lowering the pH toward the pK_a value (6.8). After the initial burst, Nap-FF then assembled continuously and more slowly, over several hours. With calcium chloride (70 μL, 5 wt %/vol), the immobilization of Nap-FF was faster than GdL-triggered assembly. This would be expected, given that $CaCl_2$-triggered assembly only relies on mixing the two components and, unlike GdL, does not require one of them to be activated by a reaction.

In fluorescence spectroscopy, exciting the naphthalene ring of Nap-FF at 280 nm leads to an emission peak at 350 nm in basic solution. When GdL was added, the peak showed a slight red shift to 355 nm, and over time, a second peak at 380 nm emerged along with a complex emission at higher wavelengths, indicative of $\pi-\pi$ stacking (Figure S13).[73,74] The fluorescence spectrum of Nap-FF triggered by $CaCl_2$ addition was broadly similar, with a new peak at ca. 380 nm emerging along with complex peaks at higher wavelengths (Figure S14). Therefore, there is evidence for $\pi-\pi$ stacking of naphthalene units in each case.

The IR spectrum of the GdL-triggered Nap-FF xerogel had a C═O stretch at 1728 cm^{-1}, consistent with protonation of the terminal carboxylic acid, as well as sharp peaks at 3421 and 3297 cm^{-1} (Figure 2b). In contrast, $CaCl_2$-triggered Nap-FF did not have a carboxylic acid C═O stretch, with C═O stretches only observed at lower wavenumbers, where they can be assigned to amides and the deprotonated carboxylate (Figure 2b). The N−H and O−H stretches were also significantly broadened. These major differences prove that the gels assemble from different species depending on the triggering mechanism. On GdL-triggering, the terminal carboxylate group is protonated, whereas, on calcium ion addition, the terminal carboxylate instead forms calcium salt bridges,[67] with both mechanisms leading to gel formation.

Circular dichroism (CD) spectroscopy indicated that when Nap-FF (0.01 wt %/vol) was mixed with GdL and left to stand for 24 h, the CD spectrum displayed a positive band at ca. 240 nm corresponding to the $\pi-\pi^*$ transition of the aromatic phenyl group (Figure S18).[75] A large negative band at ca. 220 nm corresponds to GdL.[76] In addition, there is a negative peak at ca. 200 nm, which would suggest some fibers adopt random coils.[75] We also used HCl as an alternative acid source to trigger assembly, removing the GdL signal from the CD spectrum (Figure S19). This emphasized the large positive peak (now centered at ca. 225 nm due to the removal of GdL)

https://doi.org/10.1021/acs.chemmater.4c00183
Chem. Mater. XXXX, XXX, XXX−XXX

and the negative peak at ca. 200 nm remained. On triggering with $CaCl_2$, the CD spectrum of Nap-FF has a large positive peak at 245 nm and a large negative peak at 210 nm (Figure S20). The calcium-triggered CD spectrum is therefore significantly different from that of the acid-triggered system, suggesting a different nanoscale Nap-FF assembly mode (see further discussion below).

Fiber growth kinetics were also followed by recording CD spectra every 10 min for 2.5 h and at 24 h. On GdL addition to Nap-FF (0.02 wt %/vol), the CD spectrum slowly evolved over 24 h into protonated assembled Nap-FF (Figure S21). On addition of calcium ions, nanoscale assembly was rapid, with the CD bands being present from the beginning of the experiment, followed by a slight increase in ellipticity over time (Figure S22).

Overall, the spectroscopic evidence makes clear that the choice of trigger leads to two different modes of Nap-FF assembly on the molecular scale, which occur with different rates, both underpinned by $\pi-\pi$ stacking of the aromatic naphthalene units but with one based on carboxylic acid protonation and the other by salt bridges, leading to different nanoscale chiral organization.

Transmission electron microscopy (TEM) indicated that in the basic solution, Nap-FF formed worm-like micelles, with some spherical aggregates also being observed (Figure S23). When assembled using GdL, Nap-FF formed β-sheets with a fiber width of 5−25 nm (Figures 2c, S24, and S28). Scanning electron microscopy (SEM) also indicated a sheet-like assembled morphology (Figures 2d and S30). In contrast, for calcium ion triggering, TEM indicated the formation of long bundles with much better defined diameters of 5−10 nm (Figures 2e, S25, and S28). It is often the case in supramolecular gels that the morphologies visualized by electron microscopy have dimensions larger than the molecular scale.[77] This is a result of the bundling of individual fibrils—indeed fibril−fibril interactions play a key role in the hierarchical assembly process of the overall gel. In this case, the observed morphologies presumably result from calcium ion bridges between long worm-like micelles.[46,67] SEM imaging indicated the formation of an interpenetrated fibrillar nanoscale network for $CaCl_2$-triggered Nap-FF (Figures 2f and S31), different from the sheet-like assemblies visualized for GdL-triggered Nap-FF.

On the macroscopic level, gel thermal stability was assessed by tube inversion methodology. The T_{gel} value of Nap-FF (0.3 wt %/vol) triggered by GdL was ca. 68 °C, and for Nap-FF (0.3 wt %/vol) triggered by $CaCl_2$, it was 64 °C—relatively similar values (Tables S1 and S2). In terms of rheological performance, however, the G' values of the GdL-triggered gel (Figures S36 and S37) and the Ca^{2+}-triggered gel (Figures S41 and S42) were 9770 and 2430 Pa, respectively, indicating that triggering with $CaCl_2$ gave rise to a softer gel. This is consistent with the different morphologies observed by SEM, with the sheet-like GdL-triggered network forming a stiffer matrix.

In summary (Table 1), Nap-FF forms effective gels with both GdL and $CaCl_2$ triggers. These gels have different molecular-scale assembly modes and assembly kinetics, which lead to different nanoscale networks and rheological behaviors.

Multicomponent Gels Triggered by GdL or $CaCl_2$. Having characterized Nap-FF gels formed with different triggers, we then combined them with thermally responsive DBS-$CONHNH_2$. To form the GdL-triggered two-component gel, a suspension of DBS-$CONHNH_2$ was mixed with a basic aqueous solution of Nap-FF, heated to dissolve DBS-$CONHNH_2$, transferred to a vial containing known quantities of GdL (0.8 wt %/vol), and left overnight. A gel formed relatively quickly as the DBS-$CONHNH_2$ cooled. This gel then slowly became more translucent as the Nap-FF assembled. To form the $CaCl_2$-triggered two-component gel, a suspension of DBS-$CONHNH_2$ was mixed with basic aqueous Nap-FF, heated until it dissolved, transferred to a vial containing known quantities of calcium chloride (70 μL, 5 wt %/vol), and left overnight. A transparent gel formed relatively quickly.

Table 1. Summary of Difference between GdL-Triggered Assembly and $CaCl_2$-Triggered Assembly

GdL-triggered gel	$CaCl_2$-triggered gel
slower assembly kinetics	faster assembly kinetics
CO_2H-based gel	$CO_2^-\cdots Ca^{2+}$-based gel
sheet-like assembly (5−25 nm)	bundle assembly (5−10 nm)
stiffer gel (G' = 9770 Pa)	softer gel (G' = 2430 Pa)

^{1}H NMR spectroscopy indicated that for the GdL-triggered multicomponent gel, the ^{1}H NMR peaks of DBS-$CONHNH_2$ disappeared from the spectrum even at a concentration of 0.15 wt %/vol, well below its usual minimum gelation concentration (MGC) of 0.28 wt %/vol (Figure S7). This indicates that DBS-$CONHNH_2$ is assembling into a solid-like network below its normal MGC. This suggests that GdL-triggered assembly of Nap-FF promotes DBS-$CONHNH_2$ assembly. This could result from a degree of molecular-scale coassembly or the two networks supporting one another's assembly on the nanoscale (see below).

We then followed the assembly of the two gel networks over time (Figure S9). Using a GdL trigger, >90% of the two gelators were assembled into their networks, and the rate of assembly of Nap-FF was similar to DBS-$CONHNH_2$ (i.e., <1 min for most to assemble). Interestingly, Nap-FF was immobilized faster in the presence of DBS-$CONHNH_2$ than it was on its own, presumably because the use of an increased temperature to trigger the DBS-$CONHNH_2$ hydrogel led to an increased rate of GdL hydrolysis.

To determine whether the two networks could be individually addressed, we investigated disassembly and reassembly of the Nap-FF network in the presence of DBS-$CONHNH_2$ (Figure 3). First, NaOD (0.5 M, 40 μL) was added on top of the multicomponent gel to deprotonate Nap-FF. After 72 h, ^{1}H NMR indicated that approximately 73% of the Nap-FF network had been converted into the mobile solution phase. Conversely, only slight solubilization of DBS-$CONHNH_2$ (ca. 7%) was observed. This suggests a degree of self-sorting on the molecular scale between LMWGs—if they were coassembled at the molecular level, the base-induced disassembly of Nap-FF would cause DBS-$CONHNH_2$ to also disassemble.[78] The Nap-FF was then reassembled via subsequent acidification by adding GdL (8 mg in 0.1 mL D_2O), resulting in 100% of Nap-FF network reformation (5 days). This process took extended periods of time for diffusion of triggers due to the small diameter of the NMR tube. In summary, the assembly and disassembly of the Nap-FF network in the presence of assembled DBS-$CONHNH_2$ indicates that on the molecular scale, the LMWGs assemble mostly independently of one another.

For the $CaCl_2$-triggered gel, when Nap-FF (0.15 wt %/vol) was combined with DBS-$CONHNH_2$ (0.3 wt %/vol) and $CaCl_2$, the two gelators both assembled very quickly, with

https://doi.org/10.1021/acs.chemmater.4c00183
Chem. Mater. XXXX, XXX, XXX−XXX

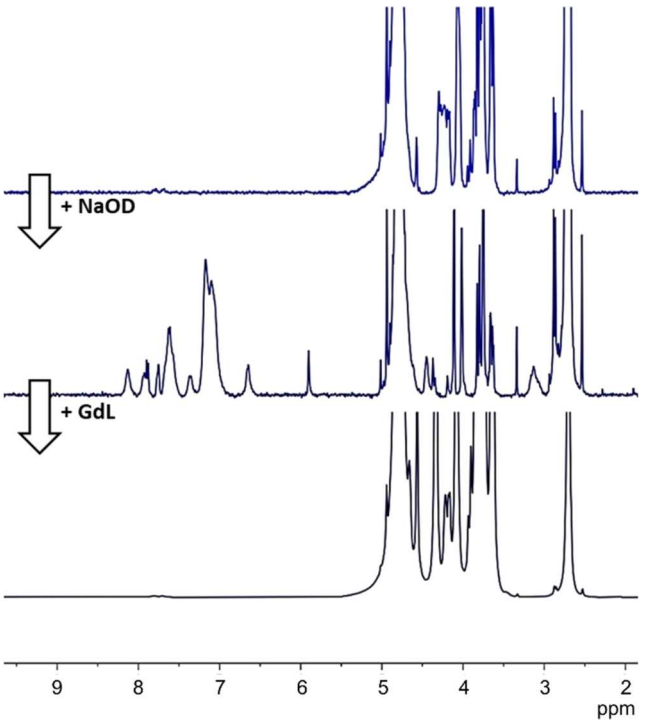

Figure 3. ^{1}H NMR spectra of GdL-triggered DBS-$CONHNH_2$/Nap-FF gel (0.3 wt %/vol of DBS-$CONHNH_2$ and 0.15 wt %/vol of Nap-FF) after NaOD addition leading to Nap-FF disassembly and subsequent GdL addition to reassemble the Nap-FF network.

some evidence that assembly was complete for Nap-FF more quickly than for DBS-$CONHNH_2$, although the time scales were too fast to resolve this by NMR (Figures S8 and S10). Nap-FF was immobilized faster in the presence of DBS-$CONHNH_2$ than in its absence, which we assign to the use of heating in the multicomponent system accelerating mixing and calcium binding.

Using CD spectroscopy, we could see that the multicomponent gels with both GdL and $CaCl_2$ triggers had CD spectra that were approximately the sum of the CD spectra for the individual assembled gels, consistent with a model in which the two LMWGs form assemblies that are largely self-sorted on the molecular scale (Figures S18−S20).

Fiber growth kinetics were followed by recording CD spectra every 10 min for 2.5 h and at 24 h. After GdL addition to DBS-$CONHNH_2$/Nap-FF (0.02 wt %/vol each), the evolution of the CD spectrum (Figure S21) was slower than in the absence of DBS-$CONHNH_2$. Nonetheless, over time, the expected end-point was reached, in which the CD spectrum appeared as a combination of individual spectra. For $CaCl_2$ triggering (Figure S22), the kinetics of nanofiber formation were faster and were similar in the presence or absence of DBS-$CONHNH_2$. All of these processes are kinetically slower than the NMR study described above because the system is significantly below the MGC.

Fluorescence spectroscopy of GdL-triggered multicomponent Nap-FF/DBS-$CONHNH_2$ gels indicated an emission peak at 380 nm (Figure S13). However, the expected peak for DBS-$CONHNH_2$ at 350 nm was not observed. This is consistent with emission being primarily from self-assembled Nap-FF and suggests that some energy transfer from DBS-$CONHNH_2$ to Nap-FF takes place. For the $CaCl_2$-triggered multicomponent gel, the fluorescence spectrum was similar but with a slightly lower intensity (Figure S14).

Infrared spectroscopy indicated that for the GdL-triggered gel, the spectrum broadly corresponded to an overlap of the two individual spectra (Figure S15). However, the peak assigned to the C═O of the terminal COOH group of Nap-FF showed a shift of the O−H stretch shifted from ca. 3298 to 3288 cm^{-1} and also some small changes in the C═O stretch at higher Nap-FF concentrations. This suggests noncovalent interactions between the −COOH and −$CONHNH_2$ groups in these multicomponent xerogels. Although NMR makes clear that on the molecular level, the components are largely independent and can be separately assembled and disassembled; IR therefore suggests that interactions between these functional groups might be responsible for fiber−fiber interactions at the nanoscale level. These would encourage DBS-$CONHNH_2$ to assemble even below its MGC, as observed with GdL-triggering. In the case of the $CaCl_2$-triggered gel, the IR spectrum of the multicomponent system was equivalent to the sum of the individual components (Figures S16 and S17). This indicates, in agreement with the other studies, that when using calcium triggering, the two components self-sort into nanoscale networks that are essentially independent of one another.

TEM studies on the GdL-triggered multicomponent gel (Figures 4a, S26, and S28) indicated a combination of the β-sheets (5−25 nm) of Nap-FF (Figure 2c) and the long twisted nanofibers (5−30 nm), consistent with DBS-$CONHNH_2$ (TEM imaging of DBS-$CONHNH_2$ alone confirming this assignment has been published previously).[27,79] This observation therefore directly supports self-sorting at the molecular level, with the two gelators each forming their own independent nanoscale morphologies. Interestingly, however, when using SEM to visualize the network-level assembly, although sheet-like Nap-FF assemblies were observed, they were more densely packed and interlinked, suggestive of a supporting, interactive role being played by DBS-$CONHNH_2$ (Figures 4c and S32). This is consistent with the view that although on the molecular level, these gelators self-sort into their own assemblies, on the network level, there are interactions between them. For the $CaCl_2$-triggered gels, TEM visualized two different thicknesses of fiber (Figures 4b, S27, and S28). Based on the imaging of these two gelators when taken individually, we can assign the thinner fibers (5−10 nm) as being distinctive of $CaCl_2$-triggered Nap-FF (Figure 2e) and the thicker fibers (15−30 nm) as corresponding to DBS-$CONHNH_2$ (TEM imaging of DBS-$CONHNH_2$ alone has been previously reported).[27,79] TEM imaging of these multicomponent systems therefore provides clear evidence of orthogonal self-sorted assembly.

SEM imaging demonstrated the presence of branched entangled nanofibers interpenetrated with one another—differences between fibers could not easily be visualized by SEM owing to their similarity (Figure 4d); however unlike when using a GdL trigger, there was no evidence of nanoscale network-level interactions between them.

The thermal stability of the GdL- and $CaCl_2$-triggered multicomponent gels (0.3 wt %/vol of each component) was >100 °C, indicating enhanced thermal stability and suggesting that in both cases, the two systems combine at the network level to yield a material with enhanced thermal stability (Tables S1 and S2). However, when creating multicomponent gels using DBS-$CONHNH_2$ below its MGC (0.15 wt %/vol of

https://doi.org/10.1021/acs.chemmater.4c00183
Chem. Mater. XXXX, XXX, XXX−XXX

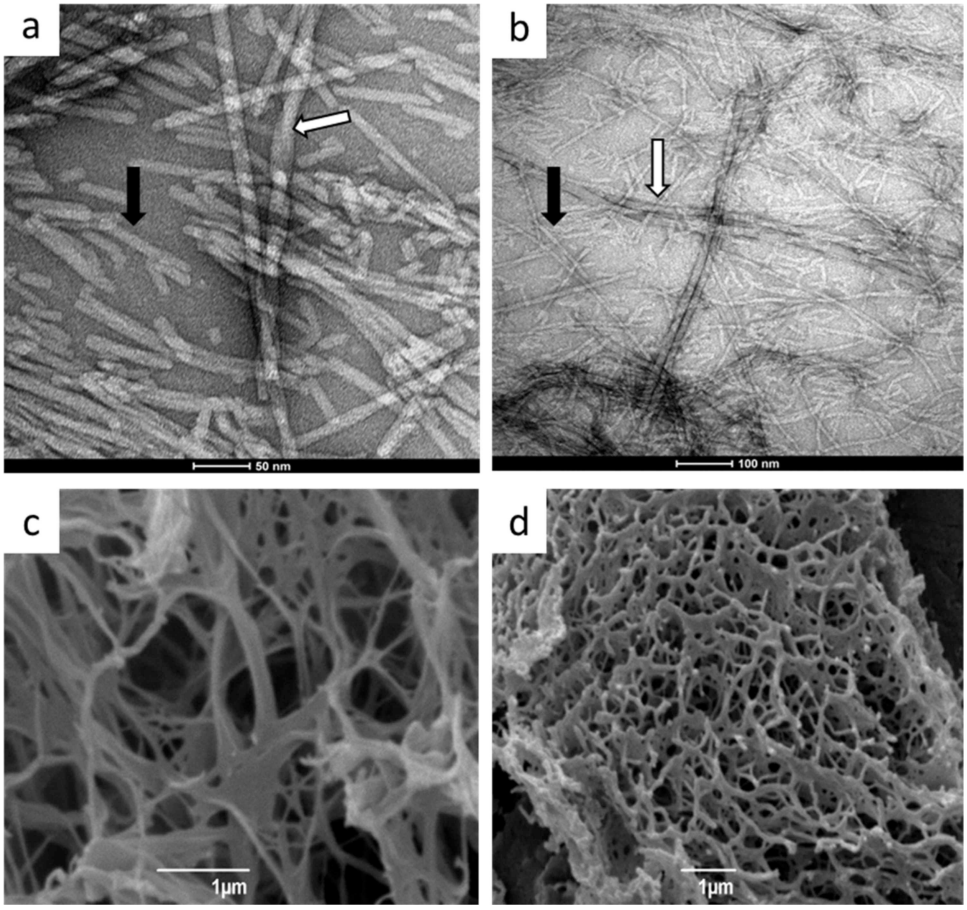

Figure 4. (a) TEM image of Nap-FF/DBS-CONHNH$_2$ triggered by GdL: black arrow highlights Nap-FF, white arrow highlights DBS-CONHNH$_2$, and scale bar = 50 nm; (b) TEM image of Nap-FF/DBS-CONHNH$_2$ triggered by $CaCl_2$, black arrow highlights Nap-FF, white arrow highlights DBS-CONHNH$_2$, and scale bar = 100 nm; (c) SEM image of Nap-FF/DBS-CONHNH$_2$ triggered by GdL, scale bar = 1 μm; and (d) SEM image of Nap-FF/DBS-CONHNH$_2$ triggered by $CaCl_2$, scale bar = 1 μm.

Table 2. Rheological Performance of Gels as Determined via Amplitude Sweep at 25 °C Using a 20 mm Parallel Plate and a Gap of 2.5 mm at a Frequency of 1 Hz

gel	trigger	Nap-FF loading (%)	DBS-CONHNH$_2$ loading (%)	G'/Pa	G''/Pa	yield stress (%) ($G' = G''$)
DBS-CONHNH$_2$			0.3	940	75	5.1
Nap-FF	GdL	0.3		9770	700	6.4
Nap-FF	GdL	0.5		15,140	1270	5.0
two-component	GdL	0.15	0.15	2445	145	10.1
two-component	GdL	0.3	0.3	7495	730	10.1
two-component	GdL	0.5	0.3	26,230	2085	4.0
Nap-FF	$CaCl_2$	0.3		2430	240	10.0
Nap-FF	$CaCl_2$	0.5		6195	700	12.6
two-component	$CaCl_2$	0.15	0.15	815	95	12.7
two-component	$CaCl_2$	0.3	0.3	5870	710	13.1
two-component	$CaCl_2$	0.5	0.3	10,640	1240	17.6

each component), the GdL-triggered system has significantly greater thermal stability (74 °C) than the $CaCl_2$-triggered system (56 °C). This, once again, supports the view that when triggered by GdL, Nap-FF can support/promote the assembly of DBS-CONHNH$_2$, whereas when triggered by $CaCl_2$, it cannot.

Rheology (Table 2) found that for the GdL-triggered two-component gel (0.3 wt %/vol of each gelator), the G' value was 7500 Pa—intermediate between DBS-CONHNH$_2$ (940 Pa) and GdL-triggered Nap-FF (9770 Pa) (Figure S39). This suggests a combination of rheological properties of the two networks reflecting their mutual interaction to form a new sample-spanning material. Relatively stiff gels (G' = 2450 Pa) were still formed even when DBS-CONHNH$_2$ was below its MGC (both components 0.15 wt %/vol) (Figure S38). On increasing Nap-FF loading to 0.5%, the gels became stiffer and resistance to shear (yield stress) decreased (Figure S40), consistent with the presence of a larger number of more rigid self-assembled sheet-like nanostructures within the gel.

When triggered by $CaCl_2$, the two-component gel had a G' value of 5870 Pa, above the individual G' values for DBS-CONHNH$_2$ (940 Pa) and $CaCl_2$-triggered Nap-FF (2430 Pa),

https://doi.org/10.1021/acs.chemmater.4c00183
Chem. Mater. XXXX, XXX, XXX−XXX

suggestive of a combination of the two independent networks to form an interpenetrated gel (Figures S43−S45). However, it was below the G' value of the equivalent GdL-triggered multicomponent gel, in agreement with the lower thermal stability and the different nanoscale morphology observed by TEM. Using GdL gives a β-sheet type assembly which would reasonably be expected to be stiffer than the bundles of fibrils produced by $CaCl_2$. However, all of the $CaCl_2$-triggered hydrogels were more resistant to strain, consistent with the less rigid, more adaptive nanostructure.

In summary, therefore (Figure 5), the multicomponent system differs depending on whether it is triggered by GdL or

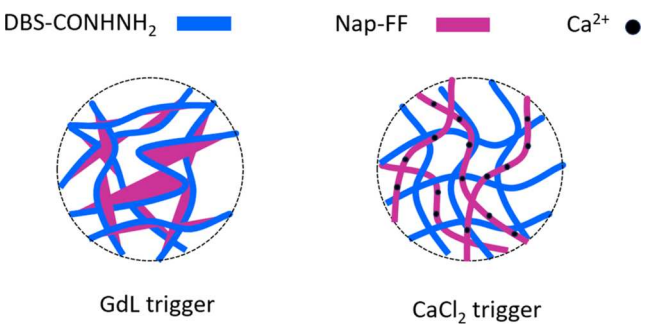

Figure 5. Schematic diagram summarizing the different assembly modes of multicomponent gels depending on the choice of trigger.

$CaCl_2$. In both cases, it would appear that the LMWGs self-sort on the molecular level into their nanoscale assemblies. However, the sheet-like Nap-FF assemblies induced by GdL encourage the assembly of DBS-$CONHNH_2$ below its MGC, and the two assemblies interact with one another on a network level as a result of hydrogen bond interactions between the acylhydrazide and the carboxylic acid. Conversely, when using a $CaCl_2$ trigger, the two networks are independent of one another on the network level—the carboxylic acid is bound to calcium in the form of its carboxylate salt, and therefore it cannot interact with DBS-$CONHNH_2$. In this way, the molecular structures that underpin gel assembly are able to dictate the type of self-sorting that takes place.

Patterning Dynamic Multidomain Gels via Ca^{2+} Diffusion. Having gained an understanding of this multicomponent system, we then moved onto shaping and patterning it. Previously, we have explored patterning multicomponent gels by acid diffusion,[62−64] demonstrating it is a powerful approach to generating dynamic multidomain gels with evolving and/or transient spatially resolved characteristics. Although studies in which H^+ diffusion is used to trigger gelation are increasingly common,[56−64] very few studies have investigated the diffusion of other active species in order to trigger gel formation.[54,55,80−82] Having demonstrated that $CaCl_2$ was an effective alternative trigger for multicomponent systems, yielding fully characterized self-sorted multicomponent gels across all length scales, we next decided to explore whether calcium ions could be used as a mild, diffusible trigger to pattern these multicomponent gels. The goal was to achieve spatial and temporal control of Nap-FF assembly by diffusing $CaCl_2$ within a preformed DBS-$CONHNH_2$ matrix.

For the initial studies, Nap-FF (0.3 wt %/vol) in water (6.5 mL total volume) was dissolved in NaOH (0.5 M, 1.3 equiv) and then transferred to a 14 mL vial containing DBS-$CONHNH_2$ (0.3 wt %/vol) in the presence of bromothymol blue as an indicator. The mixture was subsequently heated to fully dissolve the DBS-$CONHNH_2$, giving a clear blue solution. The hot solution was transferred to a 3.5 cm Petri dish and allowed to cool to room temperature. After the DBS-$CONHNH_2$ gel was formed, we used an optimized process to inject calcium chloride into the gel. To inject a $CaCl_2$ solution (2 M, 15 μL), the position of the gel in the Petri dish was controlled by a lab jack while the calcium ion solution loaded in a glass syringe was injected (Figure 1c). This technique left a loading puncture mark equal to the needle size, with all of the solution going into the gel, and no leakage back out onto the gel surface. This achieves $CaCl_2$ loading with minimal disruption to the gel matrix—a significant improvement on our previous diffusion work, which instead cut reservoirs into the preformed gel to load diffusing species.[62,63]

After the solution of $CaCl_2$ was injected into the preformed network of DBS-$CONHNH_2$ that contains the basic solution of Nap-FF, a yellow-green ring expanded from the injection point over time, indicating slight pH lowering on diffusion of calcium ions (Figure S1). There was no color change when the same amount of water was injected instead of calcium chloride solution (Figure S2). Changing the pH-indicator to thymol blue gave a clearer visual observation of the calcium ion diffusion process (Figures S3 and S4). We assumed that the growth of this ring indicated the formation of Nap-FF network, as the calcium ions cross-link carboxylate groups, forming the Nap-FF network. However, beyond the indicated color change, we could not actually observe the Nap-FF gel being assembled in the preformed DBS-$CONHNH_2$. The appearance of a slightly opaque region was noted, but it was not clear enough for well-defined visual observation. This is perhaps not surprising given that (as described above) the calcium-triggered Nap-FF gel is relatively transparent (unlike the H^+-triggered gel, which has considerable translucency). We therefore went on to perform experiments without the indicator present to emphasize visual changes associated with triggering Nap-FF and enable other experimental approaches to understanding patterning.

We first turned to ^{1}H NMR to confirm self-assembly was taking place. Aliquots of the gel (100 μL) were sampled at three distances from the injection point (0−5.8 mm, 5.8−11.6 mm, and 11.6−17.5 mm) using a cut plastic syringe, and transferred, with minimal disruption, to an NMR tube. DMSO was added as internal standard and the samples analyzed by ^{1}H NMR (Figures 6a, S11, and S12). Independent studies were performed in triplicate, and averages were reported. In the "inner" two regions, from the injection site out to a radius of 11.6 mm, 90−95% of Nap-FF became immobilized within the supporting DBS-$CONHNH_2$ matrix at 1−3 h and was therefore not visible in the NMR spectrum. However, in the "outer" region at a further distance of 11.6−17.5 mm from the injection site, Nap-FF was mostly mobile after the first hour, and the percentage of assembled Nap-FF then increased to ca. 20% after 3 h, 30% after 6 h, and 48% after 24 h. It is thus clear that $CaCl_2$ diffuses through the existing DBS-$CONHNH_2$ gel and induces the gelation of Nap-FF over a period of hours. Interestingly, over 24 h, as the calcium continues to diffuse outward and starts to equalize its concentration across the Petri dish, the cross-linking density and immobilized gelator in the inner regions close to the injection site begin to decrease (to ca. 75%). This indicates that the assemblies formed by calcium cross-linking are not kinetically or thermodynamically trapped and are responsive, continuing to exchange calcium

https://doi.org/10.1021/acs.chemmater.4c00183
Chem. Mater. XXXX, XXX, XXX−XXX

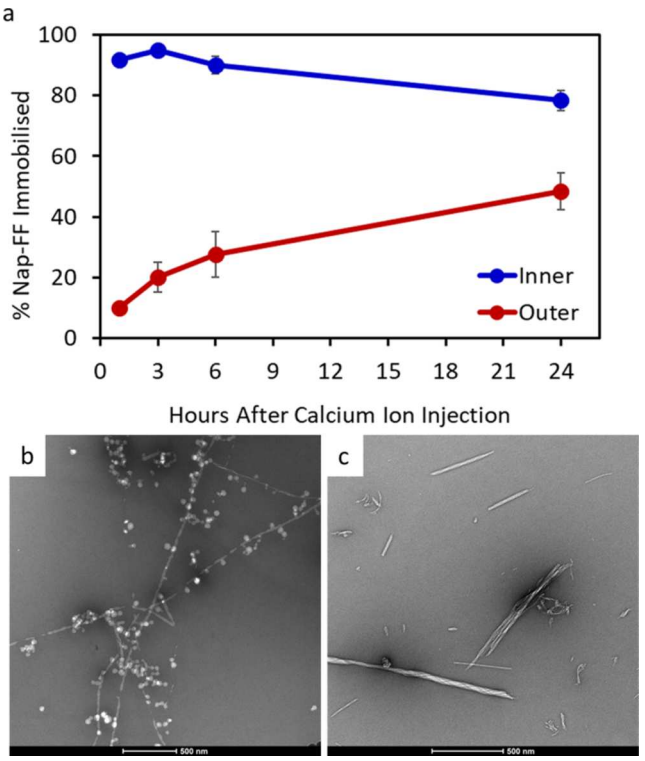

Figure 6. (a) Graph indicating the % of Nap-FF immobilized over time after injection of $CaCl_2$ solution (0.03 mmol) into a preformed DBS-$CONHNH_2$ gel, as measured by sampling and ^1H NMR spectroscopy, $N = 3$, mean reported. TEM images of (b) outer and (c) inner parts, scale bar = 500 nm in each case.

with the surrounding medium giving rise to a highly dynamic Nap-FF network.

TEM was also used to study the nanoscale structure of the inner and outer domain gels. Gel samples (12 mL, 0.3 wt %/vol of each LMWG) were prepared in 5 × 5 cm square glass trays, and the $CaCl_2$ solution (0.06 or 0.03 mmol) was injected to initiate Nap-FF assembly in opposite corners (Figure 7a). The gels were left for 2.5 h before samples from the inner and outer parts were cut using a bottomless vial. The outer and inner gel samples were handled in the same way to allow for comparison. TEM images of the outer domain (Figures 6b and S29) indicate the presence of micelles of Nap-FF. However, within the inner domain (Figures 6c and S29), which has been exposed to the diffusing $CaCl_2$, these micelles have disappeared, and Nap-FF nanofibers are instead observed, in the presence of helical DBS-$CONHNH_2$ fibers. SEM imaging indicated fibrillar networks (Figures S34 and S35).

The mechanical properties of the gels produced by diffusion were also tested on gel samples prepared in 5 × 5 cm square glass trays as described above and analyzed by rheology using a 20 mm parallel plate geometry (Figure 7b). The G' value of the sample from the inner part that had been exposed to Ca^{2+} was ca. 11400 Pa (0.03 mmol $CaCl_2$ injection) and ca. 10250 Pa (0.06 mmol $CaCl_2$ injection), within error of one another (Figures S46 and S47). These G' values are higher than for the multicomponent gel prepared in standard vials. It is important to note that the fabrication method is different here in that the DBS-$CONHNH_2$ is pre-existing, and the Nap-FF is cross-linked by calcium at room temperature, via diffusion. This should lead to slower and more complete assembly of the Nap-FF via calcium cross-linking. Most importantly, the outer parts which had not been exposed to calcium were very much softer, with a G' value of only 260 Pa (Figure S48). The G' value between domains therefore differs by almost 2 orders of magnitude. In this way, calcium diffusion is able to drive very large changes in gel stiffness, creating dynamic multidomain materials that can evolve and adapt their rheological properties over a period of hours (Figure 8).

In summary, therefore, the diffusion of calcium ions through a preformed gel of DBS-$CONHNH_2$ is a simple methodology that allows the assembly of Nap-FF to be switched on with both temporal and spatial resolution. As the second network assembles in response to the diffusing Ca^{2+} trigger, the stiffness of the gel (G' value) increases by a factor of ca. 50, creating materials in which different domains have different physical properties as they evolve over time.

CONCLUSIONS

In conclusion, we have studied multicomponent gels based on Nap-FF and DBS-$CONHNH_2$, with Nap-FF assembly being

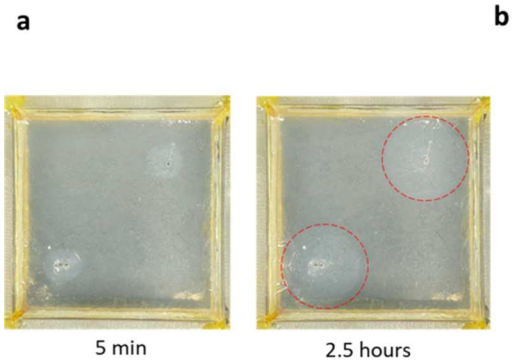

b

Gel	G' (Pa)	G" (Pa)	cross over	STD of G'	STD of G"
inner-0.03 mmol	11409	1413	10.1%	1082	84
inner-0.06 mmol	10242	1364	10.4%	608	131
outer	262	80	6.3%	85	13

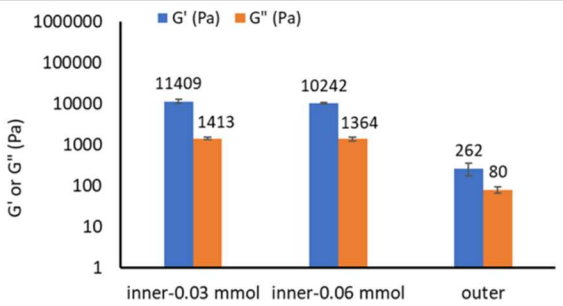

Figure 7. (a) Photographs of the DBS-$CONHNH_2$/Nap-FF gel for rheology prepared in a 5 × 5 cm tray with two injection points in bottom left and top right corners. Aliquots of the inner region (within red circles where Nap-FF assembly can just be visualized) and outer parts were cut using bottomless vials and analyzed by TEM or rheology. (b) Table and bar chart representing the rheological data from the experimental setup in panel (a). $N = 3$, mean reported.

https://doi.org/10.1021/acs.chemmater.4c00183
Chem. Mater. XXXX, XXX, XXX−XXX

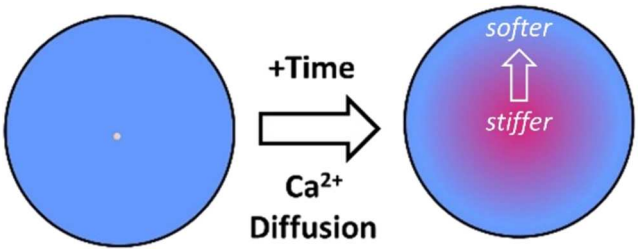

Figure 8. Schematic diagram showing calcium diffusion over time through a DBS-$CONHNH_2$ gel loaded with deprotonated Nap-FF, leading to the spatially resolved assembly of Nap-FF over time, induced by Ca^{2+} to give multidomain gels with stiffer and softer domains.

triggered either using GdL or $CaCl_2$. Changing triggers alters the way in which Nap-FF assembles on the molecular scale, which leads to different nanoscale networks and different rheological behaviors. The choice of trigger also directs the properties of the two-component gels. In both cases, the LMWGs self-sort on the molecular level into their nanoscale assemblies. However, the sheet-like Nap-FF carboxylic acid assemblies induced by GdL encourage the assembly of DBS-$CONHNH_2$. The two assemblies appear to interact with one another on a network level as a result of hydrogen bond interactions between the acylhydrazide and the carboxylic acid. Conversely, when using a $CaCl_2$ trigger, the two networks are independent of one another on the network level, presumably because the carboxylic acid is bound to calcium in the form of its carboxylate salt and therefore cannot interact with DBS-$CONHNH_2$. As such, GdL-triggering leads to molecular-level self-sorting and network-level coassembly, while $CaCl_2$-triggering leads to both molecular-level and network-level self-sorting.

By injecting calcium chloride into a preformed DBS-$CONHNH_2$ gel and using it as a diffusing trigger for Nap-FF assembly, we demonstrated that spatially resolved gels could result. These patterned multidomain gels had stiffnesses differing by 2 orders of magnitude depending on whether or not they had been exposed to the Ca^{2+} trigger. Furthermore, the patterned domains evolved over time, showing transient behavior, as the trigger diffused and ultimately began to equilibrate through the system. Given the mild, biocompatible nature of $CaCl_2$, it is suggested that this approach may have future relevance in cell-based studies in terms of patterning gels in a dynamic way to interact with growing tissue. Work toward this target is currently in progress.

■ ASSOCIATED CONTENT

Supporting Information

The Supporting Information is available free of charge at https://pubs.acs.org/doi/10.1021/acs.chemmater.4c00183.

Additional characterization data: gel fabrication photographs, NMR analysis, fluorescence, CD and IR spectra, TEM and SEM images, and rheology plots (PDF)

■ AUTHOR INFORMATION

Corresponding Author

David K. Smith − *Department of Chemistry, University of York, York YO10 5DD, U.K.;* orcid.org/0000-0002-9881-2714; Email: david.smith@york.ac.uk

Author

Chayanan Tangsombun − *Department of Chemistry, University of York, York YO10 5DD, U.K.;* orcid.org/0000-0002-8794-7533

Complete contact information is available at: https://pubs.acs.org/10.1021/acs.chemmater.4c00183

Author Contributions

The original concept was developed by D.K.S., who supervised the project. C.T. carried out all experimental work. Both authors were involved in data analysis, and the writing of the paper was led by D.K.S., with contributions from C.T.

Notes

The authors declare no competing financial interest.

■ ACKNOWLEDGMENTS

C.T. was funded by a scholarship from the Thai Government (AD039701). The authors acknowledge MChem student John Sanderson for helping develop the injection method for diffusion on a different chemical system. The authors thank Dr. Karen Hodgkinson (Department of Biology, University of York) for TEM and SEM imaging and Dr. Heather Fish (Department of Chemistry, University of York) for assistance with the NMR studies.

■ REFERENCES

(1) Smith, D. K. Supramolecular Gels—A Panorama of Low-Molecular-Weight Gelators from Ancient Origins to Next-Generation Technologies. *Soft Matter* **2023**, *20*, 10−70.

(2) Weiss, R. G. The Past, Present, and Future of Molecular Gels. What is the Status of the Field, and Where is it Going? *J. Am. Chem. Soc.* **2014**, *136*, 7519−7530.

(3) Draper, E. R.; Adams, D. J. Low-Molecular-Weight Gels: The State of the Art. *Chem* **2017**, *3*, 390−410.

(4) Jones, C. D.; Steed, J. W. Gels with Sense: Supramolecular Materials that Respond to Heat, Light and Sound. *Chem. Soc. Rev.* **2016**, *45*, 6546−6596.

(5) Panja, S.; Adams, D. J. Stimuli-Responsive Dynamic Transformations in Supramolecular Gels. *Chem. Soc. Rev.* **2021**, *50*, 5165−5200.

(6) Sangeetha, N. M.; Maitra, U. Supramolecular Gels; Functions and Uses. *Chem. Soc. Rev.* **2005**, *34*, 821−836.

(7) Hirst, A. R.; Escuder, B.; Miravet, J. F.; Smith, D. K. High-Tech Applications of Self-Assembling Supramolecular Nanostructured Gel-Phase Materials: From Regenerative Medicine to Electronic Devices. *Angew. Chem., Int. Ed.* **2008**, *47*, 8002−8018.

(8) Du, X.; Zhou, J.; Shi, J.; Xu, B. Supramolecular Hydrogelators and Hydrogels: From Soft Matter to Molecular Biomaterials. *Chem. Rev.* **2015**, *115*, 13165−13307.

(9) Shao, T.; Falcone, N.; Kraatz, H.-B. Supramolecular Peptide Gels: Influencing Properties by Metal Ion Coordination and Their Wide-Ranging Applications. *ACS Omega* **2020**, *5*, 1312−1317.

(10) Hirst, A. R.; Smith, D. K. Two-Component Gel-Phase Materials—Highly Tunable Self-Assembling Systems. *Chem. - Eur. J.* **2005**, *11*, 5496−5508.

(11) Buerkle, L. E.; Rowan, S. J. Supramolecular Gels formed from Multi-Component Low Molecular Weight Species. *Chem. Soc. Rev.* **2012**, *41*, 6089−6102.

(12) Draper, E. R.; Adams, D. J. How Should Multicomponent Supramolecular Gels be Characterised? *Chem. Soc. Rev.* **2018**, *47*, 3395−3405.

(13) Sugiyasu, K.; Kawano, S.-i.; Fujita, N.; Shinkai, S. Self-Sorting Organogels with p−n Heterojunction Points. *Chem. Mater.* **2008**, *20*, 2863−2865.

(14) Moffat, J. R.; Smith, D. K. Controlled Self-Sorting in the Assembly of 'Multi-Gelator' Gels. *Chem. Commun.* **2009**, 316−318.

(15) Singh, N.; Zhang, K.; Angulo-Pachón, C. A.; Mendes, E.; van Esch, J. H.; Escuder, B. Tandem Reactions in Self-Sorted Catalytic Molecular Hydrogels. *Chem. Sci.* **2016**, *7*, 5568−5572.
(16) Onogi, S.; Shigemitsu, H.; Yoshii, T.; Tanida, T.; Ikeda, M.; Kubota, R.; Hamachi, I. *In Situ* Real-Time Imaging of Self-Sorted Supramolecular Nanofibers. *Nat. Chem.* **2016**, *8*, 743−752.
(17) Draper, E. R.; Dietrich, B.; Adams, D. J. Self-Assembly, Self-Sorting, and Electronic Properties of a Diketopyrrolopyrrole Hydrogelator. *Chem. Commun.* **2017**, *53*, 1864−1867.
(18) Shigemitsu, H.; Fujisaku, T.; Tanaka, W.; Kubota, R.; Minami, S.; Urayama, K.; Hamachi, I. An Adaptive Supramolecular Hydrogel Comprising Self-Sorting Double Nanofibre Networks. *Nat. Nanotechnol.* **2018**, *13*, 165−172.
(19) Okesola, B. O.; Wu, Y.; Derkus, B.; Gani, S.; Wu, D.; Knani, D.; Smith, D. K.; Adams, D. J.; Mata, A. Supramolecular Self-Assembly To Control Structural and Biological Properties of Multicomponent Hydrogels. *Chem. Mater.* **2019**, *31*, 7883−7897.
(20) Chu, C.-W.; Schalley, C. A. Recent Advances on Supramolecular Gels: From Stimuli-Responsive Gels to Co-Assembled and Self-Sorted Systems. *Org. Mater.* **2021**, *3*, 25−40.
(21) Panja, S.; Dietrich, B.; Smith, A. J.; Seddon, A.; Adams, D. J. Controlling Self-Sorting versus Co-assembly in Supramolecular Gels. *ChemSystemsChem* **2022**, *4*, No. e2022000008.
(22) Li, Y.-X.; Xu, L.; Kang, S.-M.; Kang, S.; Zhou, L.; Zhou, L.; Liu, N.; Liu, N.; Wu, Z.-Q. Helicity- and Molecular-Weight-Driven Self-Sorting and Assembly of Helical Polymers towards Two-Dimensional Smectic Architectures and Selectively Adhesive Gels. *Angew. Chem., Int. Ed.* **2021**, *60*, 7174−7179.
(23) Wang, Y.; Lovrak, M.; Liu, Q.; Maity, C.; le Sage, V. A. A.; Guo, X.; Eelkema, R.; van Esch, J. H. Hierarchically Compartmentalized Supramolecular Gels through Multilevel Self-Sorting. *J. Am. Chem. Soc.* **2019**, *141*, 2847−2851.
(24) Kubota, R.; Nagao, K.; Tanaka, W.; Matsumura, R.; Aoyama, T.; Urayama, K.; Hamachi, I. Control of Seed Formation allows Two Distinct Self-Sorting Patterns of Supramolecular Nanofibers. *Nat. Commun.* **2020**, *11*, No. 4100.
(25) Nakamura, K.; Kubota, R.; Aoyama, T.; Urayama, K.; Hamachi, I. Four Distinct Network Patterns of Supramolecular/Polymer Composite Hydrogels Controlled by Formation Kinetics and Interfiber Interactions. *Nat. Commun.* **2023**, *14*, No. 1696.
(26) Adams, D. J. Personal Perspective on Understanding Low Molecular Weight Gels. *J. Am. Chem. Soc.* **2022**, *144*, 11047−11053.
(27) Okesola, B. O.; Smith, D. K. Versatile Supramolecular pH-tolerant Hydrogels which Demonstrate pH-dependent Selective Adsorption of Dyes from Aqueous Solution. *Chem. Commun.* **2013**, *49*, 11164−11166.
(28) Piras, C. C.; Mahon, C. S.; Genever, P. G.; Smith, D. K. Shaping and Patterning Supramolecular Materials—Stem Cell-Compatible Dual-Network Hybrid Gels Loaded with Silver Nanoparticles. *ACS Biomater. Sci. Eng.* **2022**, *8*, 1829−1840.
(29) Piras, C. C.; Kay, A. G.; Genever, P. G.; Fitremann, J.; Smith, D. K. Self-Assembled Gel Tubes, Filaments and 3D-Printing with in situ Metal Nanoparticle Formation and Enhanced Stem Cell Growth. *Chem. Sci.* **2022**, *13*, 1972−1981.
(30) Piras, C. C.; Smith, D. K. Sequential Assembly of Mutually Interactive Supramolecular Hydrogels and Fabrication of Multi-Domain Materials. *Chem. - Eur. J.* **2019**, *25*, 11318−11326.
(31) Houton, K. A.; Morris, K. L.; Chen, L.; Schmidtmann, M.; Jones, J. T. A.; Serpell, L. C.; Lloyd, G. O.; Adams, D. J. On Crystal versus Fiber Formation in Dipeptide Hydrogelator Systems. *Langmuir* **2012**, *28*, 9797−9806.
(32) Cross, E. R.; Adams, D. J. Probing the Self-Assembled Structures and pK_a of Hydrogels Using Electrochemical Methods. *Soft Matter* **2019**, *15*, 1522−1528.
(33) Tang, C.; Smith, A. M.; Collins, R. F.; Ulijn, R. V.; Saiani, A. Fmoc-Diphenylalanine Self-Assembly Mechanism Induces Apparent pK_a Shifts. *Langmuir* **2009**, *25*, 9447−9453.
(34) Chen, L.; Revel, S.; Morris, K.; Serpell, L. C.; Adams, D. J. Effect of Molecular Structure on the Properties of Naphthalene−Dipeptide Hydrogelators. *Langmuir* **2010**, *26*, 13466−13471.
(35) Fleming, S.; Ulijn, R. V. Design of Nanostructures Based on Aromatic Peptide Amphiphiles. *Chem. Soc. Rev.* **2014**, *43*, 8150−8177.
(36) Raymond, D. M.; Nilsson, B. L. Multicomponent Peptide Assemblies. *Chem. Soc. Rev.* **2018**, *47*, 3659−3720.
(37) Makam, P.; Gazit, E. Minimalistic Peptide Supramolecular Co-Assembly: Expanding the Conformational Space for Nanotechnology. *Chem. Soc. Rev.* **2018**, *47*, 3406−3420.
(38) Chibh, S.; Mishra, J.; Kour, A.; Chauhan, V. S.; Panda, J. J. Recent Advances in the Fabrication and Biomedical Applications of Self-Assembled Dipeptide Nanostructures. *Nanomedicine* **2021**, *16*, 139−163.
(39) Li, L.; Xie, L.; Zheng, R.; Su, R. Self-Assembly Dipeptide Hydrogel: The Structure and Properties. *Front. Chem.* **2021**, *9*, No. 739791.
(40) Hamley, I. W. Self-Assembly, Bioactivity, and Nanomaterials Applications of Peptide Conjugates with Bulky Aromatic Terminal Groups. *ACS Appl. Bio Mater.* **2023**, *6*, 384−409.
(41) Tao, K.; Wu, H.; Adler-Abramovich, L.; Zhang, J.; Fan, X.; Wang, Y.; Zhang, Y.; Tofail, S. A. M.; Mei, D.; Li, J.; Gazit, E. Aromatic Short Peptide Architectonics: Assembly and Engineering. *Prog. Mater. Sci.* **2024**, *142*, No. 101240.
(42) Morris, K. L.; Chen, L.; Raeburn, J.; Sellick, O. R.; Cotanda, P.; Paul, A.; Griffiths, P. C.; King, S. M.; O'Reilly, R. K.; Serpell, L. C.; Adams, D. J. Chemically Programmed Self-Sorting of Gelator Networks. *Nat. Commun.* **2013**, *4*, No. 1480.
(43) Draper, E. R.; Eden, E. G.; McDonald, T. O.; Adams, D. J. Spatially Resolved Multicomponent Gels. *Nat. Chem.* **2015**, *7*, 848−852.
(44) Panja, S.; Dietrich, B.; Shebanova, O.; Smith, A. J.; Adams, D. J. Programming Gels Over a Wide pH Range Using Multicomponent Systems. *Angew. Chem., Int. Ed.* **2021**, *60*, 9973−9977.
(45) Marshall, L. J.; Bianco, S.; Ginesi, R. E.; Doutch, J.; Draper, E. R.; Adams, D. J. Investigating Multigelator Systems Across Multiple Length Scales. *Soft Matter* **2023**, *19*, 4972−4981.
(46) Chen, L.; Pont, G.; Morris, K.; Lotze, G.; Squires, A.; Serpell, L. C.; Adams, D. J. Salt-Induced Hydrogelation of Functionalised-Dipeptides at High pH. *Chem. Commun.* **2011**, *47*, 12071−12073.
(47) Shi, J.; Gao, Y.; Zhang, Y.; Pan, Y.; Xu, B. Calcium Ions to Cross-Link Supramolecular Nanofibers to Tune the Elasticity of Hydrogels over Orders of Magnitude. *Langmuir* **2011**, *27*, 14425−14431.
(48) McEwen, H.; Du, E. Y.; Mata, J. P.; Thordarson, P.; Martin, A. D. Tuning Hydrogels through Metal-Based Gelation Triggers. *J. Mater. Chem. B* **2017**, *5*, 9412−9417.
(49) Fu, W.; Farhadi Sabet, Z.; Liu, J.; You, M.; Zhou, H.; Wang, Y.; Gao, Y.; Li, J.; Ma, X.; Chen, C. Metal Ions Modulation of the Self-Assembly of Short Peptide Conjugated Nonsteroidal Anti-Inflammatory Drugs (NSAIDs). *Nanoscale* **2020**, *12*, 7960−7968.
(50) Zhang, Y.-L.; Chang, R.; Duan, H.-Z.; Chen, Y.-X. Metal Ion and Light Sequentially Induced Sol−Gel−Sol Transition of a Responsive Peptide-Hydrogel. *Soft Matter* **2020**, *16*, 7652−7658.
(51) Jia, X.; Chen, J.; Xu, W.; Wang, Q.; Wei, X.; Ma, Y.; Chen, F.; Zhang, G. Molecular Dynamics Study of Low Molecular Weight Gel Forming Salt-Triggered Dipeptide. *Sci. Rep.* **2023**, *13*, No. 6328.
(52) Chivers, P. R. A.; Smith, D. K. Shaping and Structuring Supramolecular gels. *Nat. Rev. Mater.* **2019**, *4*, 463−478.
(53) Primo, G. A.; Mata, A. 3D Patterning within Hydrogels for the Recreation of Functional Biological Environments. *Adv. Funct. Mater.* **2021**, *31*, No. 2009574.
(54) Lovrak, M.; Hendriksen, W. E. J.; Maity, C.; Mytnyk, S.; van Steijn, V.; Eelkema, R.; van Esch, J. H. Free-Standing Supramolecular Hydrogel Objects by Reaction-Diffusion. *Nat. Commun.* **2017**, *8*, No. 15317.
(55) Lovrak, M.; Hendriksen, W. E.; Kreutzer, M. T.; van Steijn, V.; Eelkema, R.; van Esch, J. H. Control over the Formation of

https://doi.org/10.1021/acs.chemmater.4c00183
Chem. Mater. XXXX, XXX, XXX−XXX

Supramolecular Material Objects by Reaction-Diffusion. *Soft Matter* **2019**, *15*, 4276−4283.
(56) Ziemecka, I.; Koper, G. J. M.; Olive, A. G. L.; van Esch, J. H. Chemical-Gradient Directed Self-Assembly of Hydrogel Fibers. *Soft Matter* **2013**, *9*, 1556−1561.
(57) Spitzer, D.; Marichez, V.; Formon, G. J. M.; Besenius, P.; Hermans, T. M. Surface-Assisted Self-Assembly of a Hydrogel by Proton Diffusion. *Angew. Chem., Int. Ed.* **2018**, *57*, 11349−11353.
(58) Thomson, L.; Schweins, R.; Draper, E. R.; Adams, D. J. Creating Transient Gradients in Supramolecular Hydrogels. *Macromol. Rapid Commun.* **2020**, *41*, No. 2000093.
(59) Maity, I.; Sharma, C.; Lossada, F.; Walther, A. Feedback and Communication in Active Hydrogel Spheres with pH Fronts: Facile Approaches to Grow Soft Hydrogel Structures. *Angew. Chem., Int. Ed.* **2021**, *133*, 22711−22720.
(60) Fan, X.; Walther, A. Autonomous Transient pH Flips Shaped by Layered Compartmentalization of Antagonistic Enzymatic Reactions. *Angew. Chem., Int. Ed.* **2021**, *60*, 3619−3624.
(61) Andriamiseza, F.; Peters, S.; Roux, C.; Dietrich, N.; Coudret, C.; Fitremann, J. Wet Spinning and 3D Printing of Supramolecular Hydrogels in Acid-Base and Dynamic Conditions. *Colloids Surf., A* **2023**, *673*, No. 131765.
(62) Schlichter, L.; Piras, C. C.; Smith, D. K. Spatial and Temporal Diffusion-Control of Dynamic Multi-Domain Self-Assembled Gels. *Chem. Sci.* **2021**, *12*, 4162−4172.
(63) Cooke, H. S.; Schlichter, L.; Piras, C. C.; Smith, D. K. Double Diffusion for the Programmable Spatiotemporal Patterning of Multi-Domain Supramolecular Gels. *Chem. Sci.* **2021**, *12*, 12156−12164.
(64) Tangsombun, C.; Smith, D. K. Fabricating Shaped and Patterned Supramolecular Multigelator Objects via Diffusion-Adhesion Gel Assembly. *J. Am. Chem. Soc.* **2023**, *145*, 24061−24070.
(65) Adams, D. J.; Morris, K.; Chen, L.; Serpell, L. C.; Bacsa, J.; Day, G. M. The Delicate Balance Between Gelation and Crystallisation: Structural and Computational Investigations. *Soft Matter* **2010**, *6*, 4144−4156.
(66) Chen, L.; Morris, K.; Laybourn, A.; Elias, D.; Hicks, M. R.; Rodger, A.; Serpell, L.; Adams, D. J. Self-Assembly Mechanism for a Naphthalene−Dipeptide Leading to Hydrogelation. *Langmuir* **2010**, *26*, 5232−5242.
(67) Chen, L.; McDonald, T. O.; Adams, D. J. Salt-Induced Hydrogels from Functionalised-Dipeptides. *RSC Adv.* **2013**, *3*, 8714−8720.
(68) Draper, E. R.; McDonald, T. O.; Adams, D. J. A Low Molecular Weight Hydrogel with Unusual Gel Aging. *Chem. Commun.* **2015**, *51*, 6595−6597.
(69) Draper, E. R.; Adams, D. J. Controlling the Assembly and Properties of Low-Molecular-Weight Hydrogelators. *Langmuir* **2019**, *35*, 6506−6521.
(70) Martin, A. D.; Wojciechowski, J. P.; Robinson, A. B.; Heu, C.; Garvey, C. J.; Ratcliffe, J.; Waddington, L. J.; Gardiner, J.; Thordarson, P. Controlling Self-Assembly of Diphenylalanine Peptides at High pH using Heterocyclic Capping Groups. *Sci. Rep.* **2017**, *7*, No. 43947.
(71) Menger, F. M.; Venkatasubban, K. S. A Carbon-13 Nuclear Magnetic Resonance Study of Dibenzoylcystine Gels. *J. Org. Chem.* **1978**, *43*, 3413−3414.
(72) Escuder, B.; Llusar, M.; Miravet, J. F. Insight on the NMR Study of Supramolecular Gels and Its Application to Monitor Molecular Recognition on Self-Assembled Fibers. *J. Org. Chem.* **2006**, *71*, 7747−7752.
(73) Yang, Z.; Liang, G.; Ma, M.; Gao, Y.; Xu, B. Conjugates of Naphthalene and Dipeptides Produce Molecular Hydrogelators with High Efficiency of Hydrogelation and Superhelical Nanofibers. *J. Mater. Chem. B* **2007**, *17*, 850−854.
(74) Chen, L.; Revel, S.; Morris, K.; Adams, D. J. Energy Transfer in Self-Assembled Dipeptide Hydrogels. *Chem. Commun.* **2010**, *46*, 4267−4269.
(75) Laverty, G.; McCloskey, A. P.; Gilmore, B. F.; Jones, D. S.; Zhou, J.; Xu, B. Ultrashort Cationic Naphthalene-Derived Self-Assembled Peptides as Antimicrobial Nanomaterials. *Biomacromolecules* **2014**, *15*, 3429−3439.
(76) Jia, G.; Qiu, S.; Li, G.; Zhou, J.; Feng, Z.; Li, C. Alkali-Hydrolysis of D-Glucono-delta-lactone Studied by Chiral Raman and Circular Dichroism Spectroscopies. *Sci. China, Ser. B: Chem.* **2009**, *52*, 552−558.
(77) Yu, G.; Yan, X.; Han, C.; Huang, F. Characterization of Supramolecular Gels. *Chem. Soc. Rev.* **2013**, *42*, 6697−6722.
(78) Drew, E. N.; Piras, C. C.; Fitremann, J.; Smith, D. K. Wet-Spinning Multi-Component Low-Molecular-Weight Gelators to Print Synergistic Soft Materials. *Chem. Commun.* **2022**, *58*, 11115−11118.
(79) Patterson, A. K.; El-Qarra, L. H.; Smith, D. K. Chirality-Directed Hydrogel Assembly and Interactions with Enantiomers of an Active Pharmaceutical Ingredient. *Chem. Commun.* **2022**, *58*, 3941−3944.
(80) Ruíz-Olles, J.; Smith, D. K. Diffusion Across a Gel−Gel Interface—Molecular-Scale Mobility of Self-Assembled 'Solid-Like' Gel Nanofibres in Multi-Component Supramolecular Organogels. *Chem. Sci.* **2018**, *9*, 5541−5550.
(81) Chen, R.; Das, K.; Cardona, M. A.; Gabrielli, L.; Prins, L. J. Progressive Local Accumulation of Self-Assembled Nanoreactors in a Hydrogel Matrix through Repetitive Injections of ATP. *J. Am. Chem. Soc.* **2022**, *144*, 2010−2018.
(82) Wang, H.; Fu, X.; Gu, G.; Bai, S.; Li, R.; Zhong, W.; Guo, X.; Eelkema, R.; van Esch, J. H.; Cao, Z.; Wang, Y. Dynamic Growth of Macroscopically Structured Supramolecular Hydrogels through Orchestrated Reaction-Diffusion. *Angew. Chem., Int. Ed.* **2023**, *62*, No. e202310162.

https://doi.org/10.1021/acs.chemmater.4c00183
Chem. Mater. XXXX, XXX, XXX−XXX